Remote Sensing of Environment 222 (2019) 119–132

Contents lists available at ScienceDirect

Remote Sensing of Environment

journal homepage: www.elsevier.com/locate/rse

Evolution of sinkholes over Wink, Texas, observed by high-resolution optical and SAR imagery

Jin-Woo Kim[a,*], Zhong Lu[a], James Kaufmann[b]

[a] Roy M. Huffington Department of Earth Sciences, Southern Methodist University, Dallas, TX, USA
[b] US Geological Survey, Rolla, MO, USA

ARTICLE INFO

Keywords:
Wink sinkholes
Aerial photography
High-resolution InSAR
Rapid subsidence
Fractures
Ground fissures

ABSTRACT

Two caprock and cover collapse sinkholes, Wink Sinks #1 and #2, in Winkler County, Texas, collapsed in 1980 and 2002, respectively. They are located in a region underlain by the Salado Formation on the eastern edge of the Delaware Basin. The sinkhole collapses were associated with intense hydrocarbon drilling and production activities in the Hendrick oilfield. Production records and prior investigations imply the sinkholes developed after salt dissolution due to freshwater intrusion, cavity formation, roof failure, and successive upward cavity migration. High-resolution (1 m) aerial photography shows the ensuing expansion of Wink Sink #2 from 2002 through 2010 and relative stability of the ground surface after 2010. Very high-resolution (25 cm) staring spotlight mode TerraSAR-X reveals the spatiotemporal details of Wink sinkhole deformations. The vicinities around the two existing sinkholes (Wink Sinks #1, #2) deformed at a rate of 5 cm/yr in line-of-sight (LOS) direction from October 2015 to March 2016, and the deformation was possibly caused by the gradual deposit of the debris from overlying unconsolidated Alluvium and Santa Rosa sandstones infilling the cavity after the sinkhole collapse. Specifically, the largest deformation of 53 cm/yr in LOS direction was found 1 km east of Wink Sink #2. Our study suggests that severe drought in 2011 widened and created fractures as well as ground fissures in the rocks overlying and underlying the salt formation due to the increased effective stress. Fractures, ground fissures, and the abandoned unplugged boreholes or improperly completed wells opened one or more vertical pathways of freshwater from groundwater flow and precipitation toward the salt bed, finally causing the rapid salt dissolution and the opening of new cavities. To explain the onset of a rapid subsidence near the Wink sinkholes, our study considers the combined effect of natural perturbation (i.e., drought, rock fractures, ground fissures, subsurface drainage, precipitation) and anthropogenic effects (i.e., improper well control). Our method to explore high-resolution imagery can be applied to characterize the sinkhole deformation and mitigate sinkhole-related geohazards.

1. Introduction

Sinkholes are depressions in the ground surface that form where subsurface drainage has removed rock or sediment to form a void (Gutiérrez et al., 2014). Though sinkholes can develop anywhere, they are most common in karst which is underlain by soluble rocks such as carbonates (primarily limestone and dolomite), evaporites (gypsum and halite), and other soluble soils and rocks. Karst is characterized by efficient underground drainage and forms most commonly in areas of soluble bedrock where dissolution creates voids and flow paths. Sinkholes are one of the characteristic surface features of karst topography and occur in the form of subsidence, collapse, and suffosion (Waltham et al., 2005). Most sinkholes form naturally as a result of subsurface drainage. Water table fluctuations during drought and extreme flooding can accelerate and intensify sinkhole and collapse development (Gutiérrez et al., 2014). However, anthropogenic activities related to salt mining and/or oil production can accelerate dissolution of soluble rocks leading to void formation and sinkhole development (Johnson et al., 2003; Powers, 2003; Land, 2013). Sinkholes in the United States are widely distributed in Alabama, Florida, Kentucky, Missouri, Pennsylvania, Tennessee, and Texas with karst and pseudokarst (non-dissolving rock terrain with subsurface drainage) (Kuniansky et al., 2016). Sinkholes are considered significant geohazards, having damaged both infrastructures (roads, dams) and civilian properties, and occasionally causing casualties in specific incidents; the conservative estimate of the losses related to the sinkhole subsidence and collapses in the United

* Corresponding author at: Roy M. Huffington Department of Earth Sciences, Southern Methodist University, 3225 Daniel Avenue, Suite 207, Dallas, TX 75205, USA.
E-mail address: jinwook@smu.edu (J.-W. Kim).

https://doi.org/10.1016/j.rse.2018.12.028
Received 3 April 2018; Received in revised form 17 December 2018; Accepted 21 December 2018

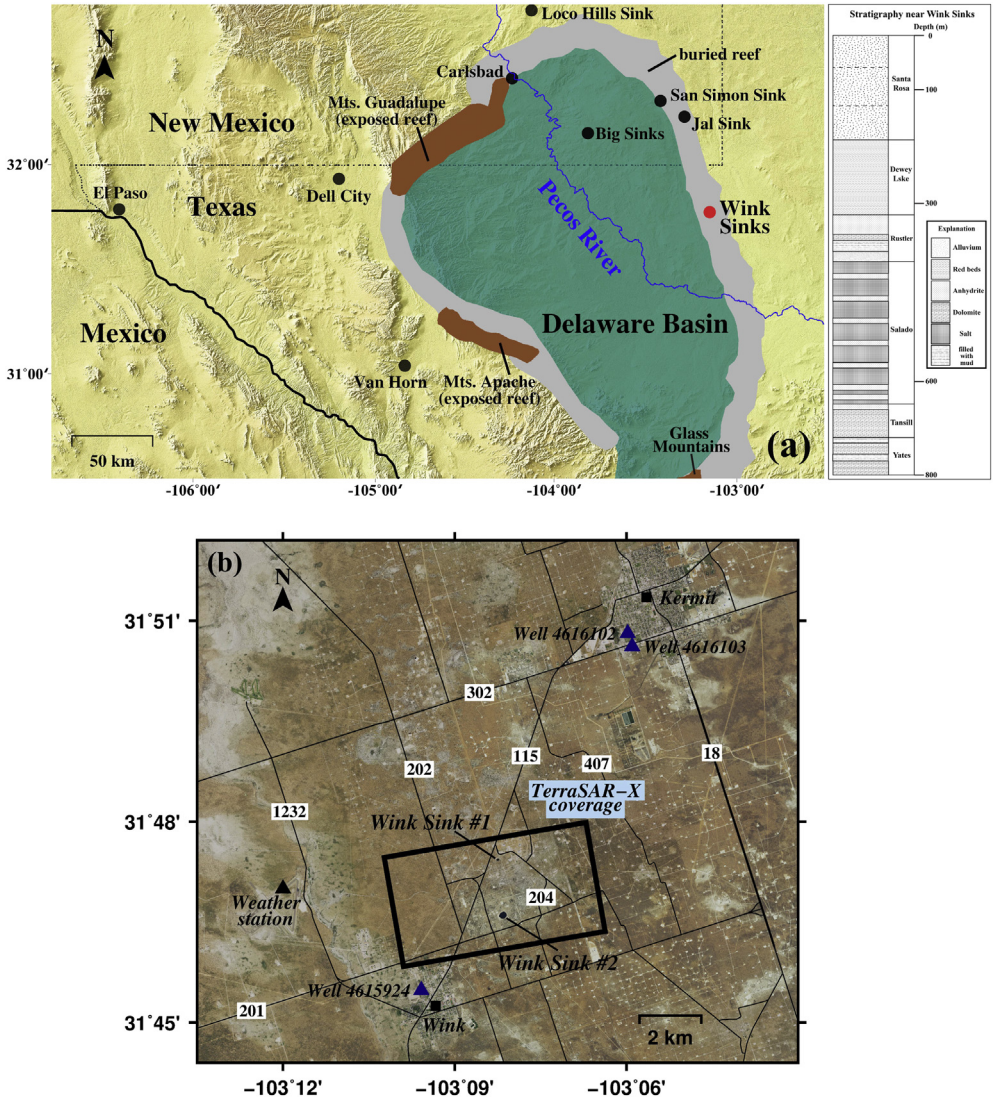

Fig. 1. (a) Delaware Basin map (background image is a shade relief map from 3-arcsec Shuttle Radar Topography Mission (SRTM) digital elevation model (DEM)). Wink Sinks developed over the buried Capitan Reef (gray shading). Stratigraphy near Wink Sinks (on the right of basin map) (Baumgardner et al., 1982; Johnson, 1989) displays the formations overlying the Capitan Reef, from Santa Rosa to Tansill and Yates Formation. (b) Coverage map (black box) of the staring spotlight mode TerraSAR-X from ascending track (background image is a NAIP image acquired in 2014). Two Wink Sinks are ~3.5 km away from Wink, Texas. One Groundwater well (4615924) is located near downtown Wink, two wells (4616102, 4616103) are near Kermit, and weather station recording precipitation is close to Winkler County Airport.

States is more than $300 million per year (Weary, 2015; Kuniansky et al., 2016).

Texas is one of the most sinkhole-prone states in the Unites States because extensive carbonate and evaporite rocks exist at or near the ground surface (Kuniansky et al., 2016). The Delaware basin of West Texas, in the southwest part of the Permian basin, contains one of the greatest accumulation of evaporites in the United States (Dean and Johnson, 1989; Kim et al., 2016). Dissolution of these evaporites has resulted in sinkhole development (Johnson, 2005). Along with natural dissolution of the evaporite rocks, human activities including oil production, water injection, and mining in salt domes can also result in ground surface deformation (e.g., Qu et al., 2015; Kim and Lu, 2018).

Many sinkholes and subsidence features are very small, < 10 m in diameter (Waltham et al., 2005). This makes it challenging to locate and quantify their subsidence phenomena. Although sinkholes and subsidence features are common in karst, their locations and description are subject to location bias (Fleury, 2009). Features impacting infrastructure or located in urban areas are more often reported by the public and local authorities than those located in more rural and vegetated areas. Remote sensing techniques, such as light detection and ranging (LiDAR), aerial photography, and SAR Interferometry (InSAR) have been employed to address these obstacles (Abelson et al., 2006; Filin et al., 2011; Panno and Luman, 2012; Zhu et al., 2014). Aerial photography and LiDAR have been utilized for mapping and characterizing sinkholes in the Dead Sea, Israel (Abelson et al., 2006; Filin et al., 2011), Kentucky, USA (Zhu et al., 2014, Zhu and Pierskalla Jr., 2016), Illinois, USA (Panno and Luman, 2012), Florida, USA (Seale et al., 2008), and Slovenia (Kobal et al., 2015). InSAR techniques, which are capable of detecting long-term precursory or ongoing deformations in major sinkhole-prone areas (Chang and Hanssen, 2014), have been used for monitoring the spatiotemporal movements of sinkholes in the Dead Sea, Israel (Baer et al., 2002; Closson et al., 2003, 2005; Nof et al., 2013; Avni et al., 2016), Bayou Corne, Louisiana, USA (Jones and Blom, 2014), New Mexico (Rucker et al., 2013), and Ebro Valley, Spain (Castañeda et al., 2009; Gutiérrez et al., 2012). The sinkholes in West Texas were initially investigated by Paine et al. (2012) using InSAR and gravimetry. Kim et al. (2016) and Kim and Lu (2018), using the spaceborne SAR satellite Sentinel-1A/B, found that the region around the two collapsed sinkholes in Wink, Texas is still subsiding and the neighboring areas of Wink Sink #2 are significantly unstable. However, the limited resolution of the airborne and spaceborne sensors used is a formidable obstacle to highly detailed measurement of the sinkhole deformation (Kim et al., 2016). Detecting localized, small deformations in collapse and subsidence sinkholes is challenging when only coarse resolution remote sensing techniques are used. The lack of high-resolution observations from space leads to a poor understanding of sinkhole development mechanisms and an inability to properly mitigate the potential geohazards.

In our study, the temporal evolution of the existing Wink sinkholes is observed by 1 m resolution aerial photography and correlated with petroleum production activities. In addition, extremely high-resolution (25 cm) SAR satellite and InSAR methods are used to monitor the current behavior of the sinkholes and neighboring region. We model the observed deformation to quantify the opening of the subsurface cavity, and investigate the spatiotemporal progress with the aid of supplementary datasets (precipitation, groundwater) and field survey. From all collected remote sensing data and hydrogeologic information, we explore the mechanisms that caused the sinkhole collapse in the past and the concurrent expansion and acceleration of sinkhole subsidence. Finally, we discuss the effects of human activities and natural perturbations on the outbreak of the ground subsidence and sinkhole occurrence where hydrocarbon has been produced intensively.

2. Study area

2.1. Characteristics of the Delaware Basin

The Delaware Basin is the western major structural sub-division of the Permian Basin of West Texas and southeastern New Mexico (Fig. 1(a)). The eastward-dipping basin contains thickly bedded evaporite sequences of the Salado and Rustler formations deposited during the Permian, and the upper Permian carbonate rocks of the Capitan Reef (gray polygons of Fig. 1(a) (Standen et al., 2009)) form the margins of the Delaware Basin (Anderson, 1981). Due to the abundant existence of evaporite and carbonate rocks, the Delaware Basin has long experienced widespread subsidence troughs, collapses and subsidence sinkholes, and breccia chimneys (e.g., carbonate caves of the Guadalupe Mountains, Big Sinks depression), all created by ongoing removal and dissolution of underlying bedded Permian salts (Anderson, 1981; Hill, 2003; Land, 2003; Warren, 2016). Moreover, a widespread depression in the inner margin of the buried Permian Capitan Reef along the eastern side of the basin has been observed (Anderson et al., 1978).

The Capitan Reef in the Delaware Basin consists of massive fossiliferous white limestone (Hiss, 1980; Hills, 1984; Warren, 2016). Due to natural dissolution induced by inflow of groundwater and intensive hydrocarbon exploration in the reef, sinkhole formation has not been uncommon over the reef in the eastern margin of the Delaware Basin; documented sinkholes include San Simon Sink and Jal (also called Whitten ranch) Sink (Anderson, 1981; Johnson et al., 2003; Powers, 2003), as well as the two Wink Sinks that collapsed in 1980 and 2002, respectively.

The sinkhole located 3.5 km northeast of Wink, Texas, called Wink Sink #1 (Fig. 1(b)), formed on 3 June 1980 near the abandoned Hendrick plugged oil well 10A, which was drilled up to 860 m depth. The well (API (American Petroleum Institute) No. 42-495-03571) produced oil from 1928 to 1951 and has been inactive since March 1964. A second sinkhole, 1.5 km south of Wink Sink #1, referred to as Wink Sink #2 (Fig. 1(b)), formed on 21 May 2002, centered on a water supply well (Gulf Water Supply (WS)-8, API No. 42-495-06415). Both sinkholes collapsed as a result of dissolution and cavity formation in the interbedded salt layer of the Salado formation (Johnson et al., 2003; Waltham et al., 2005). Evaporite dissolution, resulting in subsidence and increased basin-fill sedimentation, has been extensively observed in the Delaware Basin, and a dissolution trough also formed adjacent to the Capitan Reef (Hill, 2003; Johnson et al., 2003; Johnson, 2005). However, it has been recognized that the formation of the two Wink Sinks does not solely result from natural dissolution processes, but also from human-induced effects such as hydrocarbon production (Johnson et al., 2003; Waltham et al., 2005).

The oil exploration between Wink and Kermit in West Texas and the development of the Hendrick oilfield have a long history beginning in the 1920s. There are hundreds of oil wells within just a few kilometers of Wink Sinks #1 and #2 (Fig. 2). Currently, most of these in the immediate vicinity are abandoned and inactive (blue dots in Fig. 2), and only a small percentage of wells (red dots in Fig. 2) are active for oil and gas production and water injection.

2.2. Natural dissolution near the Wink Sinks

The natural dissolution of the Salado formation in the Delaware Basin has been long studied by numerous researchers (Ackers et al., 1930; Adams, 1944; Maley and Huffington, 1953; Hills, 1970; Bachman, 1976; Kirkland and Evans, 1976; Powers et al., 1978; Lambert, 1983; Johnson, 1986). Abnormal and abrupt thinning of the salt units with concurrent thickening of overlying rock units in the same areas was its major proof (Johnson, 1989).

Hydraulic head of water from the buried Capitan Reef is higher than that in the Tansill and Yates Formation, becoming an artesian source of freshwater and moving upward into the overlying Salado Formation (Baumgardner et al., 1982). Moreover, hydraulic head in the Santa Rosa Formation is higher than in the Dewey Lake and Rustler Formation, leading to the downward freshwater flow into the underlying Salado Formation (Baumgardner et al., 1982). Both upward and downward waterflows can possibly cause the natural dissolution of the salt beds. However, the artesian waterflow has been considered as a primary cause of a natural dissolution of the salt beds (Johnson, 1989), because there are existing fractures in the Capitan Reef, Tansill, and Yates Formation, which are created by differential compaction of sediments overlying the reef and can be conduits for freshwater under artesian pressure (Anderson and Kirkland, 1980; Baumgardner et al., 1982). On the other hand, the downward groundwater movement between upper and lower formations is impeded by the formation (Dewey Lake Formation lying between the Santa Rosa and the Salado Formation) with a relatively impermeable red-bed sequence (Fig. 1(a)). Natural dissolution due to downward freshwater movement can be very localized where the formation is fractured (Baumgardner et al., 1982). Instead, the salt dissolution due to downward freshwater movement is more likely caused by anthropogenic activities (e.g., drilling) that can fracture the formations and increase the permeability.

2.3. Fracture systems near the Wink Sinks

Fracture systems from ground surface to bottom rock formations in the Wink Sink area have been well known (Heithecker, 1932; Adams, 1944; Baumgardner et al., 1982; Johnson, 1989). When massive amounts of brines were produced during the early production stage (1930–1950) in the Hendrick Field, the principal methods for handling the great quantity of the produced water consisted of disposal in unlined, natural, and artificial earthen “evaporation” pits (Heithecker, 1932). The disposal pits in the vicinity of Wink Sinks were in fact lost through seepage into the ground. Because the ground surface consists of unconsolidated sand, gravel, silt, and clay in Cenozoic Alluvium, the oilfield brines were able to percolate down easily through the porous and permeable surface materials to reach and recharge groundwater (Johnson, 1989). Moreover, dynamite was used to blast hard rock units present in the floor of a pit (Heithecker, 1932) and the permeability of top soil (Cenozoic Alluvium) and rock (Triassic Santa Rosa) formation increased even more. Corrosion of casings by saltwater, removal of the casings upon final plugging of boreholes, and imperfect drilling and grouting can increase the permeability for downward groundwater movement between shallow aquifers and permeable strata below the salt sequence. The Salado Formation also has inherent fractures naturally caused by warping of the younger strata over the underlying Capitan Reef (Adams, 1944), by deeper solution and collapse, or by minor faulting (Baumgardner et al., 1982).

Some boreholes drilled in the vicinity of the Wink Sinks deviated too much from vertical, and field explosives were used to fracture the rock to allow boreholes to be re-aligned for increasing yield production (Vance, 1928). The explosion(s) certainly fractured the Tansill Formation and/or other rock units near the bottom of the borehole and

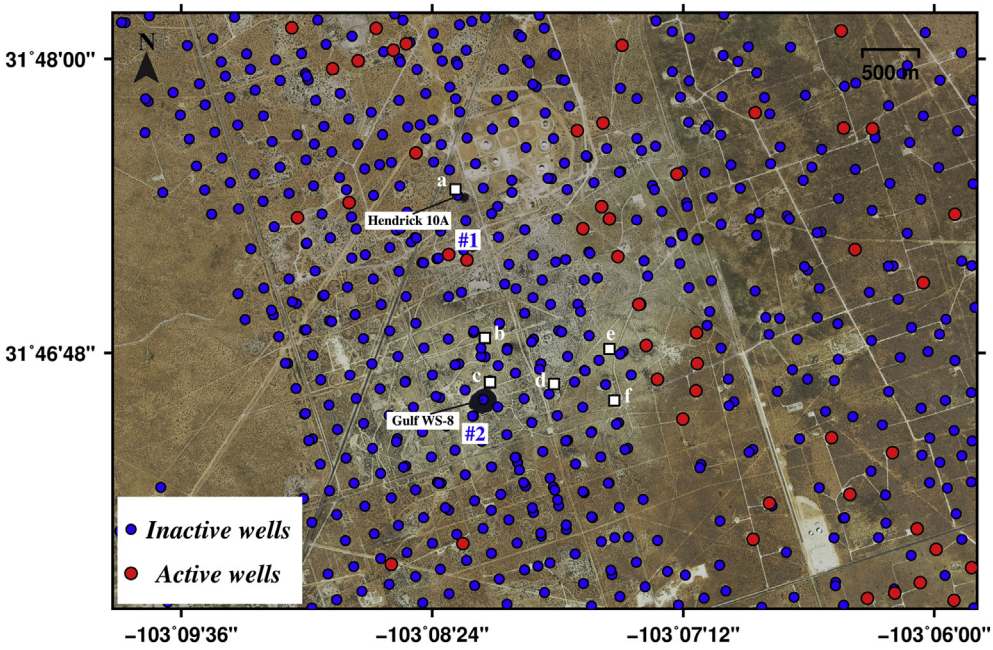

Fig. 2. Oil and gas wells around Wink Sinks. Few of them are currently active (red dots) and most wells have been inactive (blue dots) since the outcrop of two sinkholes. (For interpretation of the references to colour in this figure legend, the reader is referred to the web version of this article.)

thereby increased their permeability to circulating brines through brine-density flow (Johnson, 1989). The presence of permeable fracture systems (zones, cavities) in the Wink Sink area was evidenced by the loss of fluids during the drilling of four of the oil wells located within 1.6 km of the Wink Sinks (Baumgardner et al., 1982). One well lost circulation during drilling in sand and red beds of the Dewey Lake Formation; one well lost circulation in dolomite of the Tansill Formation; and the other two wells lost circulation during drilling in the Salado Formation (Johnson, 1989). Therefore, it is likely that the downward groundwater movement from Santa Rosa aquifer and the upward water movement under artesian pressure from the Capitan Reef and Tansill/Yates Formation are inter-connected through the fracture systems. The inter-connected water movements can inevitably accelerate the salt dissolution locally where the fracture systems are well developed.

3. Data and methods

1 m resolution aerial photography and high-resolution TerraSAR-X datasets were used to observe the temporal evolution of existing sinkholes and measure the ongoing deformation around the Wink Sinks. The National Agriculture Imagery Program (NAIP) administrated by United States Department of Agriculture (USDA) acquires aerial imagery during agricultural growing ("leaf-on") season in the contiguous United States. The aerial ortho-rectified photography over Winkler County, Texas was obtained annually or bi-annually in 2004, 2005, 2006, 2008, 2010, 2012, 2014, and 2016. Highly detailed images of 1 m spatial resolution (2 m resolution for 2005 and 2006) with Red, Green, Blue (RGB) band (Near-Infrared band is also available for 2008 dataset) can assist in delineating the collapsed regions of existing sinkholes.

Staring spotlight mode TerraSAR-X datasets were used to detect time-series deformation around the Wink Sinks. Unlike the stripmap mode SAR acquisitions that fixes the beam from the satellite antenna in the azimuth direction, the staring spotlight mode instead directly points the antenna beam to the center of the scene during whole aperture time (Kraus et al., 2016). Maximized azimuth bandwidth of a staring spotlight mode results in maximized azimuth resolution (~25 cm spatial resolution) at the expense of smaller data coverage (~5.5 km in dimension) (Carrara et al., 1995). From 16 October 2015 to 29 March 2016, 14 staring spotlight mode TerraSAR-X scenes from ascending track (Fig. S1) were acquired over the Wink Sinks, all with an 11-day interval acquisition except for 29 March 2016. The dense acquisitions with high-resolution over the sinkholes have rendered InSAR pairs with high coherence. Forty-one InSAR pairs with small (< 500 m) perpendicular baselines (Fig. S1) are used for our study. The small baseline subset (SBAS) method, capable of exploiting multi-differential interferograms with high coherence, was employed for time-series analysis (e.g., Berardino et al., 2002; Schmidt and Bürgmann, 2003; Lu and Dzurisin, 2014). The combination of all available interferograms is based on a minimum norm criterion of the velocity deformation. From observed unwrapped interferograms, the time-series (cumulative) deformation relative to the first acquisition date was estimated by inversion (Berardino et al., 2002).

Records relating to oil and gas production near the Wink sinkholes were collected from the Texas RRC (Railroad Commission), which is the responsible regulatory authority of the petroleum industry and pipeline safety in Texas. Water production information was mainly obtained from drillinginfo™, which is a service company that provides production data, reports, and analytics (i.e., oil/gas lease and permit trend). The services of both the Texas RRC and drillinginfo™ records were available by lease number, rather than by individual well. Because wells with the same lease number located near our particular well of interest are mostly controlled by the same operators, their productions are not greatly different from well to well. We therefore used the records of oil/gas and water production from the same lease number to represent those wells of our main interest.

4. Results

4.1. Past evolution of the Wink Sinks inferred from hydrocarbon production and aerial photography

4.1.1. Hydrocarbon production near the Wink Sinks

The Hendrick 10A well in the foci of the Wink Sink #1 collapse produced oil from 1928 until 1951 (Warren, 2016). While the production information for this well could not be obtained, we acquired the production information from oil wells near Wink Sink #1 (i.e., wells neighboring abandoned oil well Hendrick 3A (API No. 42-495-03561,

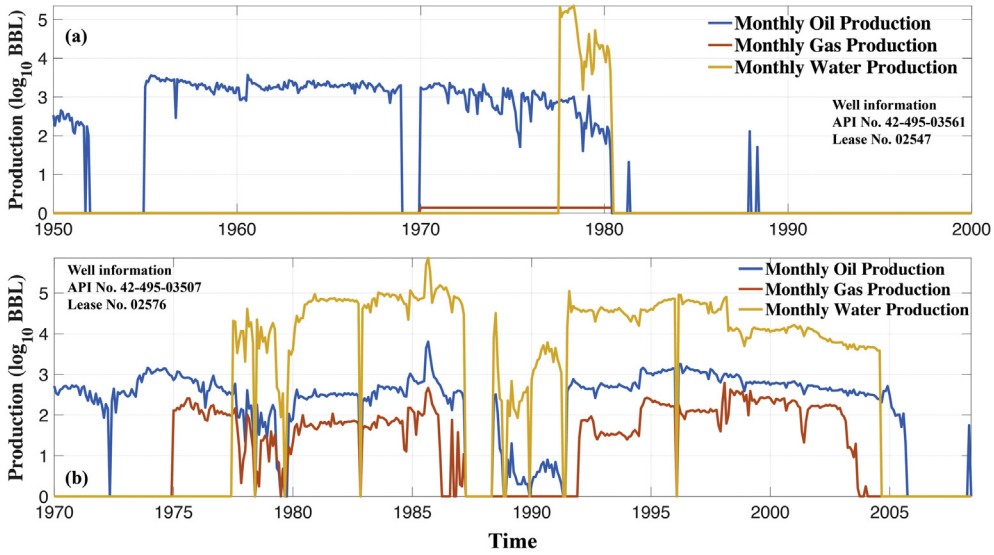

Fig. 3. Monthly oil, gas, and water production in an inactive oil (a) #1 and (b) #2 (in blue fonts of Fig. 2). (For interpretation of the references to colour in this figure legend, the reader is referred to the web version of this article.)

lease No. 02547, represented by a #1 on Fig. 2)). A review of the data provides a glimpse of what happened to the sinkhole site before and after the collapse (Fig. 3(a)). Before September 1977, dry oil containing only small amounts of sediments and water was produced, and Water to Oil Ratios (WORs) stayed near zero. However, beginning in September 1977, massive amounts of water were produced, peaking in 1978–1979. Following the collapse of Wink Sink # 1 in June of 1980, oil production at well 3A ceased. Generally, as most wells mature, the amount of water production relative to oil tends to increase, however the dramatic abrupt increase is inconsistent with the normal maturation WOR pattern. Leaks in casing, tubing, or packers can allow water from non-oil-productive zones to enter the production string, leading to an increase of water production. The high monthly WOR (once exceeding 200 in 1978) (Fig. 3(a)) seems unlikely to be induced by inappropriate well management (i.e., leaks in casing and corrosion of cement lining). Rather, it is more likely that as the reservoir near Wink Sink #1 became less productive, water flooding was implemented to stimulate the secondary oil production after the primary oil production was completed.

Because detailed production information for the Gulf WS-8 where Wink Sink #2 collapsed was not provided, we acquired the drilling, production, and completion information at wells neighboring Hendrick 13B oil well (#2 in Fig. 2; API No. 42-495-03507 with lease No. 02576) in the southwestern part of the sinkhole for comparison. Before mid-1977, oil and gas were produced without significant water production (Fig. 3(b)). However, beginning in July 1977, the water production rose, reaching a WOR of up to 800 by August 1990. Usually, when the water cut (produced water/(water + oil)) metric typically used in the petroleum industry for assessing productivity and operating condition is beyond 99%, the oil wells where water flooding has been implemented are considered economically unviable (Crabtree et al., 2000). However, the water cut exceeded the 99% level in the early 1990s and stayed at > 90% for most years. The massive water production (Fig. 3(b)) associated with water flooding operations yielding 800 million BBL in the Hendrick oilfield (Johnson et al., 2003) with inappropriate water controls at wells could have resulted in the generation of the subsurface cavity and the collapse of Wink Sink #2 in 2002. Even after Wink Sink #2 collapsed, oil production near Hendrick 13B continued until May 2008, at which time it became inactive due to the enlarged nearby sinkhole.

4.1.2. Past evolution of the Wink Sinks captured by aerial photography

Aerial photography from 2004 to 2016 (Fig. S2) shows that the collapsed region of Wink Sink #1 did not expand and the neighboring area did not change much in time, suggesting the stability of the area during that time. Even using these 1 m resolution aerial images, it is challenging to detect the ongoing subsidence around Wink Sink #1 solely based on the interpretation of optical images, and we will further examine the stability of ground surface in the Wink Sink #1 using InSAR in the later part of our study.

In contrast, Wink Sink #2 has been unstable for years. Aerial photography from 2004 to 2016 shows that ground fissures seemed to have increased for years and the collapsed region of Winks Sink #2 was enlarged (Fig. S3). Particularly, the expansion of the sinkhole between 2008 and 2010 was significant, but the growth has slowed since 2010 (Fig. S3). The expansion of sinkhole collapse over Wink Sink #2 is more obvious if time-series photographs are compared (Fig. 4(a)). The collapsed region was 38,144 ± 692 m^2 in 2004 (black dash-lined polygon in Fig. 4(a)), but it increased to 49,948 ± 792 m^2 in 2016 (red dash-lined polygon in Fig. 4(a)). The collapse area expanded as much as 30% in 10 years; the expansion was approximately linear in time from 2004 to 2010 and had been almost halted by 2010.

4.2. Status quo of Wink Sinks and neighboring region observed by high-resolution InSAR

Time-series InSAR using high-resolution staring spotlight mode TerraSAR-X imagery reveals the current status of two collapsed sinkholes (Wink Sink #1 and #2) and neighboring regions (Fig. 5). Time-series InSAR images indicate that sinkhole sites and the surrounding areas are deforming. The LOS displacement is increasing in time (Fig. 5) and the component of vertical deformation is dominant considering the characteristics of sinkhole-related ground deformation, implying that the subsidence is occurring in this area. The 25 cm resolution and dense temporal acquisition of 11 days of the staring spotlight-mode TerraSAR-X InSAR results (Fig. S1) enable us to assess the magnitude and spatial extent of deformation taking place in the sinkhole prone areas in greater detail than optical imagery.

The deformation rate map (Fig. 6(a)) from time-series InSAR measurements highlights what is occurring in the Wink sinkhole complex. Areas of deformation near Wink Sink #1 (point 'a' in Fig. 6(a)) and #2 ('c' in Fig. 6(a)) have previously been detected by other ALOS PALSAR sensor from January to July 2007 (Paine et al., 2012) and Sentinel-1A/B sensor from April to August 2015 (Kim et al., 2016; Kim and Lu, 2018). The deformation was estimated to be about 5 cm/yr, which is

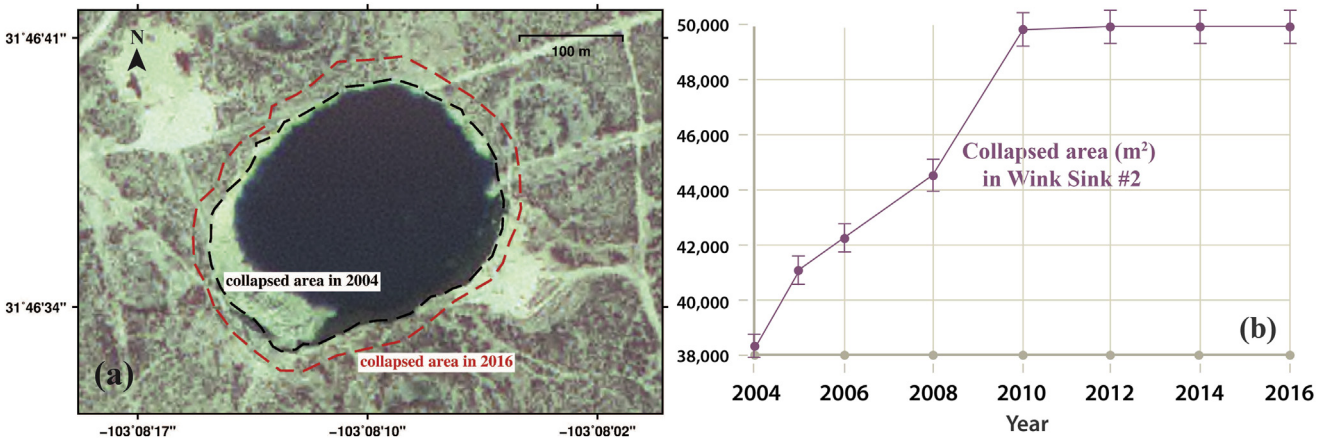

Fig. 4. (a) Collapsed area of Wink Sink #2 in 2004 (black dash-lined polygon) and 2016 (red dash-lined polygon). Background image is aerial photography taken in 2004. (b) Temporal changes of collapsed area in Wink Sink #2. (For interpretation of the references to colour in this figure legend, the reader is referred to the web version of this article.)

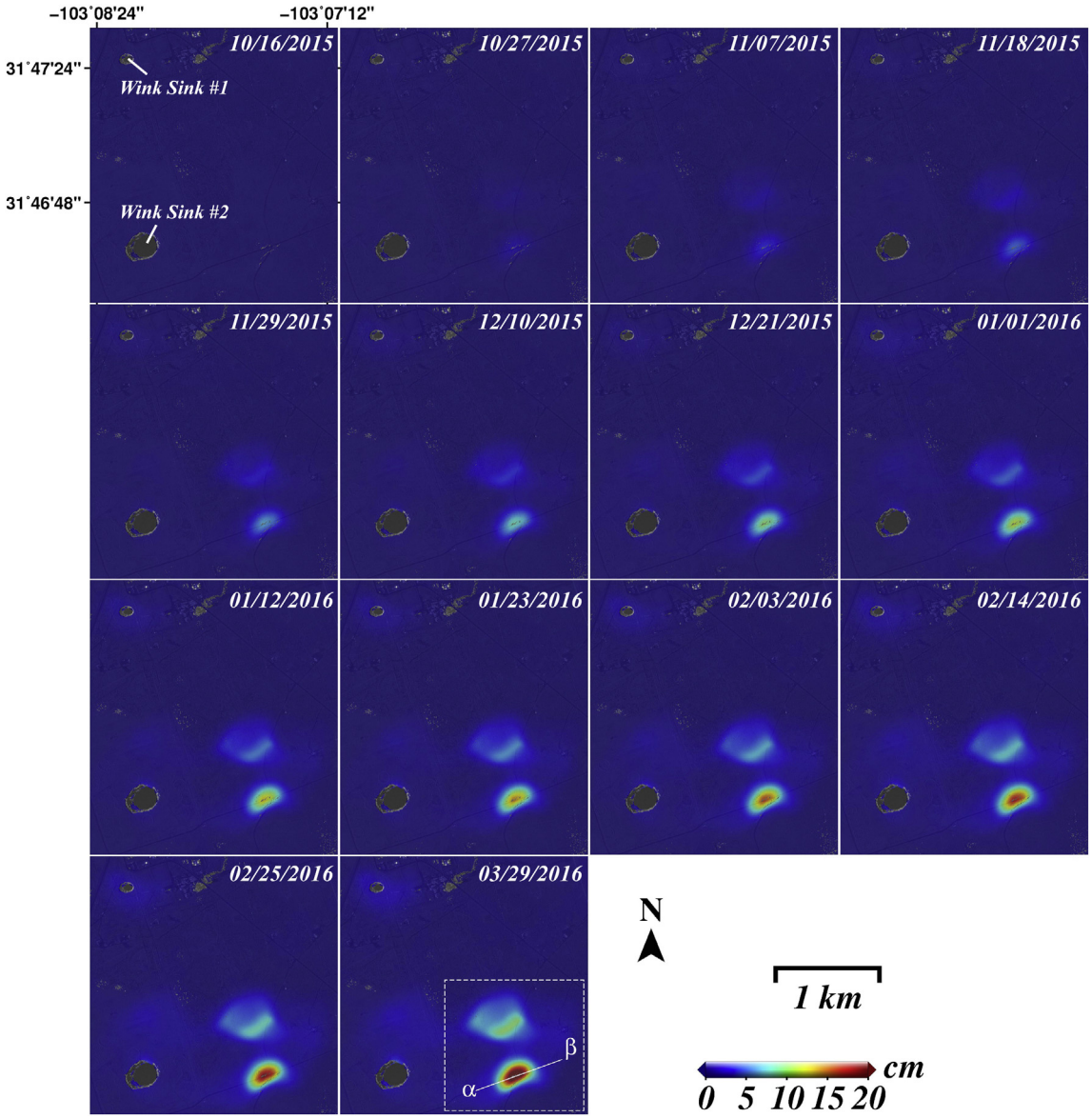

Fig. 5. Time-series deformation retrieved from staring spotlight mode TerraSAR-X between October 16, 2015 and March 29, 2016 (background image is an intensity image from staring spotlight mode TerraSAR-X). Colour represents the cumulative LOS displacement and positive values imply the increasing distance (subsidence) from SAR satellite to ground surface. The white box in the March 29, 2016 panel encompasses two subsidence bowls near Wink sinkholes.

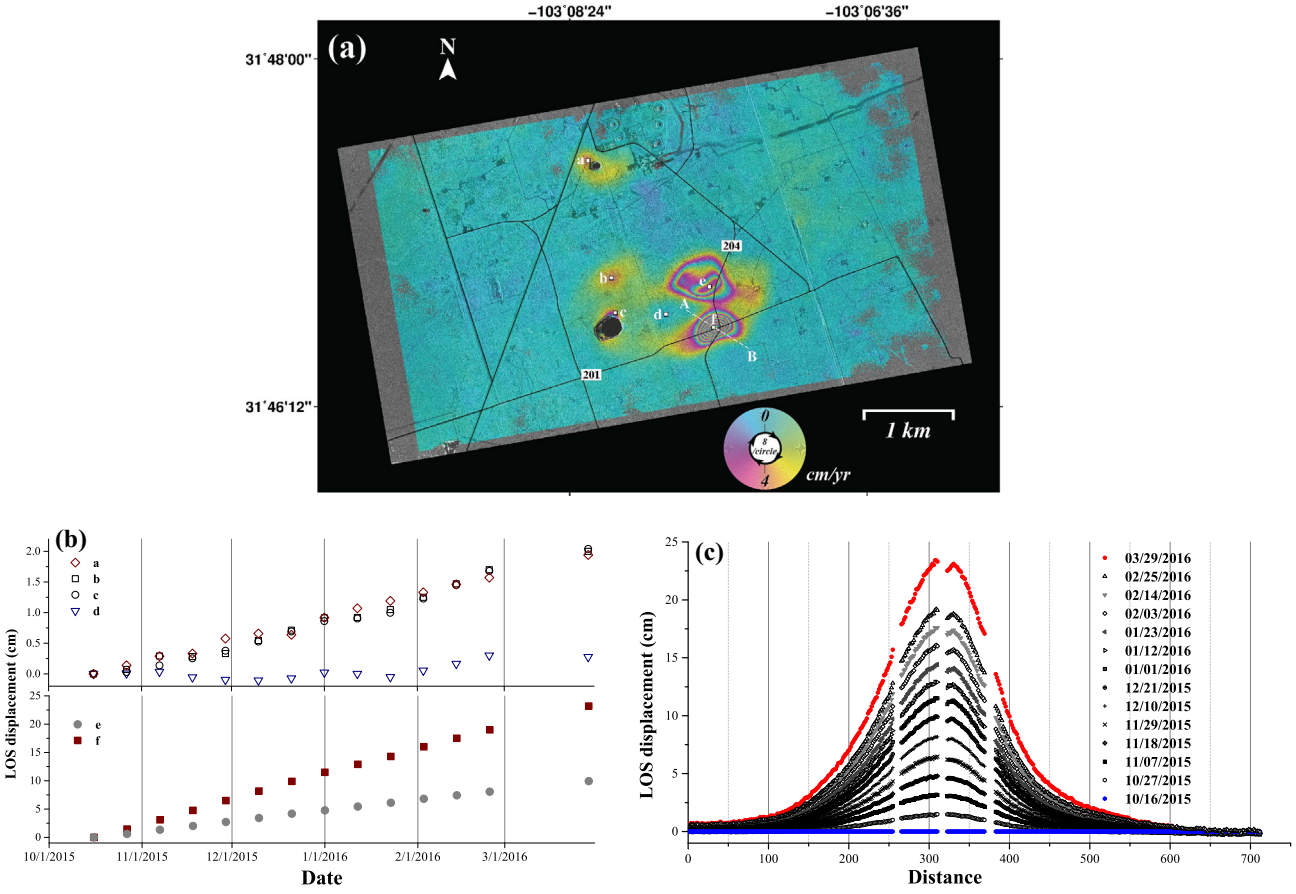

Fig. 6. (a) Deformation rate (cm/yr) around Wink Sinks in a cyclic colour pattern with 8 cm/yr interval. The maximum deformation (53 cm/yr in LOS direction) is occurring at point 'f' (intersection of County Road 201 and 204). (b) Time-series LOS displacements of a, b, c, d, e, and f and (c) time-series profile $\overline{AB}$ in Fig. 6(a).

also confirmed by our high-resolution TerraSAR-X InSAR results. The deformation indicates that both Wink Sink #1 and #2 are not stable and are still gradually expanding. While subsequent collapse of the sinkholes following their initial development has halted for now, as the time-series aerial photography affirms, the subsidence near the current sinkholes is ongoing. This can be seen as a linear trend of the accumulated deformation at points 'a' (Wink Sink #1), 'b' (300 m north of Wink Sink #2), and 'c' (Wink Sink #2) in Fig. 6(a). Each of these locations were undergoing movement in the LOS direction at a rate of nearly 5 cm/yr (2 cm LOS displacement during the 5-month period) (Fig. 6(b)). The region at 'd' in Fig. 6(a) is exhibiting a < 0.1 cm variation in LOS displacement and it is not significant compared to the other regions (Fig. 6(b)). Areas of the most concern in terms of the unstable ground surface are locations 'e' and 'f' (Fig. 6(a)), which underwent ~10 cm (23 cm/yr) and ~23 cm (53 cm/yr) between Oct 16, 2015 and Mar 29, 2016, respectively (Fig. 6(b)). The deformation in region 'e' has been previously identified using Sentinel-1A/B (Kim et al., 2016; Kim and Lu, 2018), but the signal in region 'f' could not be accurately measured by the previous InSAR methods due to the limited spatial/temporal resolutions and large gradient of displacement. The maximum subsidence (near 'f' in Fig. 6(a)) is centered on the intersection of County Road 201 and 204, and the large 430 m by 270 m oval-shaped deformation pattern implies a new cavity in the Salado Formation at ~500 m depth. The depth of sinkhole formation is inferred from that of the underlain Salado Formation in the vicinity of the Wink sinkholes (Johnson, 1989, 2005; Johnson et al., 2003). The time-series plot along profile $\overline{AB}$ in Fig. 6(b) shows the continuous increase of LOS displacement from Oct 16, 2015 to Mar 29, 2016 (Fig. 6(c)). Ground fissures at 260 m, 320 m, and 380 m distance from A are seen as non-existing points stemming from low coherence on the discontinuous ground surface. The location of ground fissures around the peak of subsidence trough can be delineated based on the low InSAR coherence points and the use of optical imagery (e.g., Google Earth™ imagery, aerial photography).

The cumulative LOS displacement over the most rapidly deforming area (white box of Fig. 5; 'e' and 'f' of Fig. 6(a)) was modeled to describe the subsurface process and, thereby, the overall subsidence pattern above the ground cavity. The model used the Okada formulation for motion on a distributed set of rectangular dislocation sources within a homogenous elastic half-space (Okada, 1985; Atzori et al., 2015; Kim et al., 2016). First, we subsampled the final cumulative LOS displacement (Fig. 7(a)) using a quadtree downsampling algorithm (Jónsson et al., 2002) to reduce the computational burden while preserving the statistically significant part of the deformation signal (Samsonov et al., 2014). The downsampling scheme reduces 510,711 pixels in the white box of Figs. 5 to 7, 469 data points in Fig. 7(a). Because two major subsidence zones are evident and a single source model did not work well (Kim et al., 2016), a two-source model was adopted. The model assumes two rectangular-shaped subsurface cavities developed in a salt layer at the fixed depth of 500 m approximately 390 m apart. The best-fitting models were searched over the grid and the best fitting parameters were defined by the root mean square (RMS) misfit from the residuals (model subtracted from observed data) (Lu and Wicks Jr., 2010; Kim et al., 2016). The best-fit model parameters of two source cavities are summarized in Table 1.

The best-fitting solution (Fig. 7(b)) has an RMS residual of 0.49 cm (Fig. 7(c)). Our model, based on a pure elastic deformation, suggests the strong possibility of two cavities in the salt formation. Although the northern cavity is larger in dimension than the southern cavity (both at the depth of 500 m where the salt dissolution is occurring), the southern

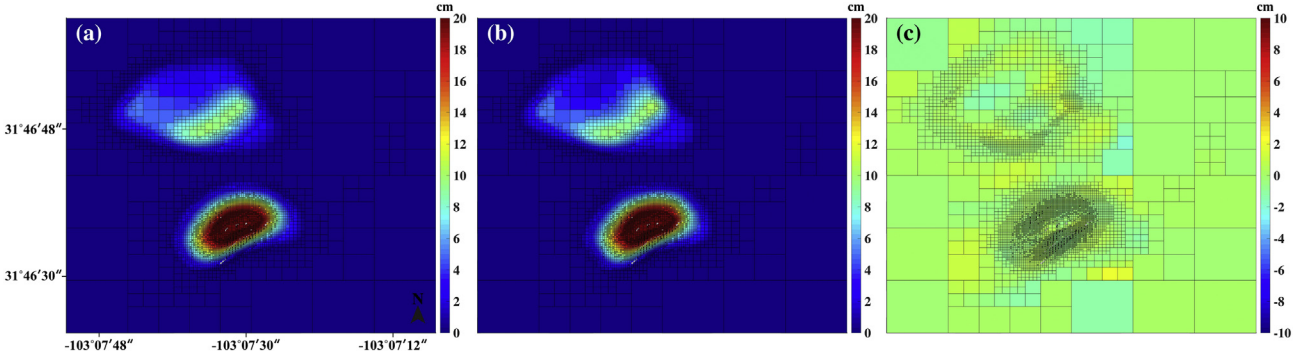

Fig. 7. (a) Cumulative LOS displacement in Mar 29, 2016 after quadtree downsampling, (b) best-fitting model based on two dislocation sources in elastic half-space, and (c) residual after subtracting the best-fitting model (b) from the cumulative deformation (a) in the box outlined in white dashed lines on the March 29, 2016 panel of Fig. 5.

cavity is undergoing larger subsidence due to more rapid salt dissolution induced by unsaturated water through fracture systems into the Salado Formation.

5. Discussion

It has been hypothesized that the collapse of Wink Sinks #1 and #2 was triggered by hydrocarbon production activities (Johnson, 1989; Warren, 2016). The procedure of drilling and completion in the Hendrick 10A well in the late 1920s and Gulf WS-8 in 1960 was consistent with past industry standards required for safe practices. However, past inappropriate borehole management in view of higher current industry standards has been suspected as a main contributor to sinkhole development. Poor sealing of the borehole and inadequate cement linings could open vertical pathways for upward (due to artesian pressure at the base of the Salado Formation) and downward (freshwater from the surface) movement of undersaturated water toward the Salado formation (Baumgardner et al., 1982). In addition, the record of water production (Fig. 3) suggests that water flooding operations contributed to the formation of both Wink sinkholes. However, the history of water production (Fig. 3) suggests that the effects of water flooding operations on the collapse of Wink Sink #2 are more predominant compared to that of Wink Sink #1. Indeed, water flooding operations in the vicinity of Wink Sink #1 lasted only 3 years, versus about 30 years in the region of Wink Sink #2. Oil production, fluid injection, and the water flooding operations can induce fractures in the producing formations, soil layers surrounding the wellbore pipes (Zoback, 2007), and above, within, and below the Salado Formation. Because the overlying insoluble soil and rocks, consisting of the sand stone and shale, collapsed into the ground cavity, the sinkhole can be classified as a caprock and cover collapse sinkhole (Waltham et al., 2005; Gutiérrez et al., 2014). After the collapsed soil and rock debris were deposited into the cavity, the bottom of the caprock sinkhole was filled with the insoluble materials. The sinkhole lake formed soon after the collapse due to the inflow from a near-surface aquifer. Despite the unconsolidated Alluvium and Santa Rosa Formation with high permeability, the water in the sinkhole lake has not been fully drained due to the effective sealing of materials filling the bottom of the collapse sinkhole.

Based solely on aerial photography (Fig. S3, Fig. 4), Wink Sink #1 appears to be more stable in terms of ongoing collapse during our observing period. On the other hand, as the debris in Wink Sink #2 continuously deposited into the cavity after the initial collapse, the lower portion of the wall has been unable to support the enlarging cavity, leading to the expansion of the collapsed sinkhole for years.

Our InSAR results detected the detailed ground deformation around Wink sinkholes that cannot be observed by aerial photography (Figs. 5, 6). The current deformation around Wink Sink #1 and #2 was is about 5 cm/yr using time-series InSAR measurements, possibly indicative of continuing mass-wasting processes in the unstable and laterally unconfined scarped margins of the collapsed sinkholes, affected by unloading cracks and topples. However, the 53 cm/yr LOS deformation rate occurring near the intersection of County Road 201 and 204 east of Wink Sink #2 is large enough to draw concerns of scientists, residents, and local authorities. Here, multiple questions are raised for this geohazard: 1) *which process initially caused such a large deformation in this area?*, 2) *Has the extent of subsidence expanded in years? and if yes,* 3) *how did the expansion happen?*.

The initial triggering mechanism for the subsidence is likely similar to that of Wink Sinks #1 and #2. Dozens of wells have been used for drilling, plugging pipes, and producing oil and gas, but most of them have been inactive and abandoned in recent years (blue dots in Fig. 8(a)). Inappropriate borehole management can initiate the freshwater contact of the Salado Formation through unplugged boreholes, corroded pipes, or leaked casing. Thirty years of water flooding operations (July 1977–July 2008) can be one important contributor to the rapid subsidence. The injected water into the producing formation (Tansill and Yates Formations) was provided by nearby water supply wells (i.e., WS10 (blue circle) in Fig. 8(a)). It is difficult to pinpoint which activity or operations are most responsible for the onset of a rapid subsidence; rather, it is likely that the combined effects of improper borehole management and water control (massive water production) created the geohazard.

In previous (Paine et al., 2012; Kim et al., 2016) and our new measurements (both from ALOS PALSAR results (personal communication with Dr. Shi) and data from TerraSAR-X), the surface expression of the subsiding area east of Wink Sink #2 significantly increased from 258,120 ± 18,010 m^2 between 2007 and 2011 (Paine et al., 2012; personal communication with Dr. Shi) (orange colored area in

Table 1
Best fit model parameters of two source cavities.

	Depth	Rectangular dimensions	Center point	Orientation azimuth
First dislocation	500 m	360 m × 100 m	31° 46′ 48″ N, 103° 7′ 36.12″ W	N20°W
Second dislocation (red area of Fig. 7(a))	500 m	315 m × 105 m	31° 46′ 35.76″ N, 103° 7′ 31.8″ W	N10°W

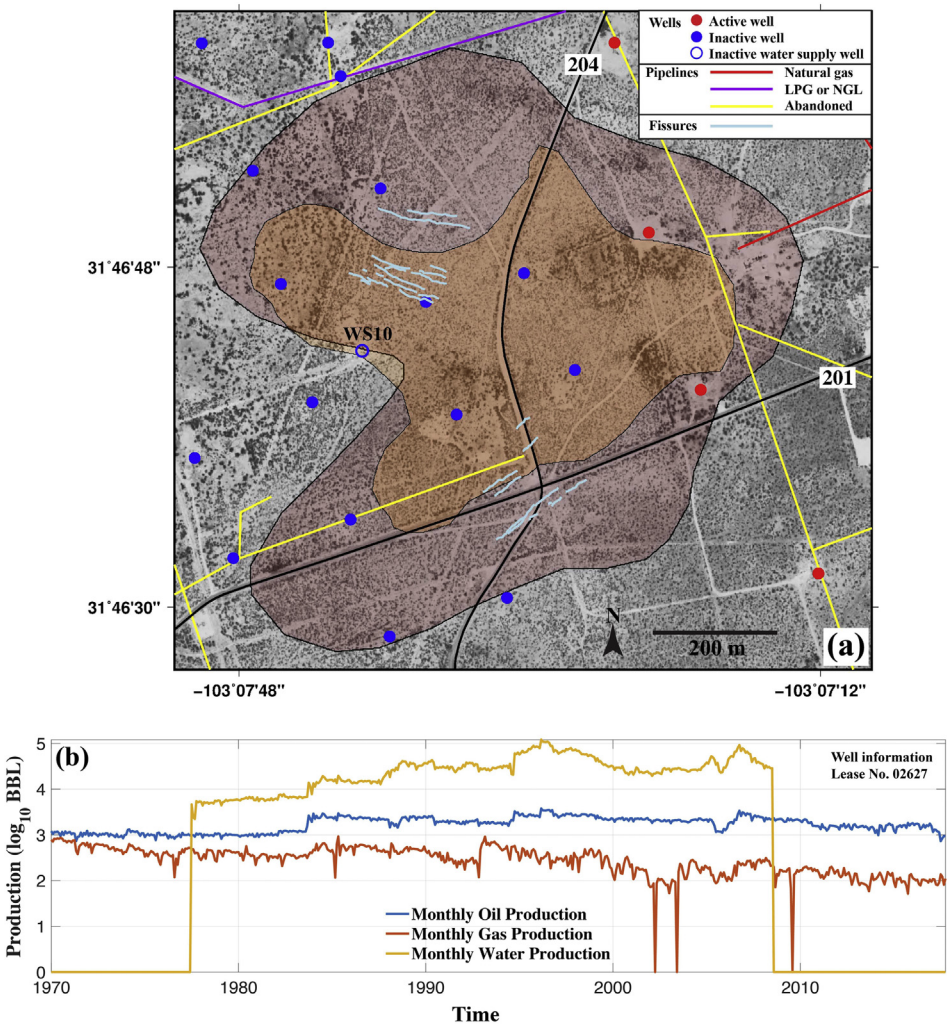

Fig. 8. (a) Subsiding areas east of Wink Sink #2. Shaded areas represent affected area detected by TerraSAR-X (brown, 609,622 ± 2768 m^2 in 2016) and ALOS PALSAR (orange, 258,120 ± 18,010 m^2 between 2007 and 2011). Neighboring wells are indicated by dots: active wells (red), inactive wells (solid blue) and an inactive water supply well (blue circle). Pipelines are shown with colored lines: buried natural gas (red), liquefied petroleum gas (LPG) or natural gas liquids (NGL) (purple), and abandoned pipelines (yellow). Ground fissures identified by InSAR coherence and Google Earth™ imagery are drawn in a light blue. (b) Monthly oil, gas, and water production in active wells (Lease No. 02627; three red dots in Fig. 8(a)). (For interpretation of the references to colour in this figure legend, the reader is referred to the web version of this article.)

Fig. 8(a)) to 609,622 ± 2768 m^2 in 2016 (brown colored area in Fig. 8(a)). Until 2011, the maximum subsiding area was restrained above County Road 201. However, the current subsidence has expanded to the south across County Road 201. The surface area of the subsiding zone as well as the maximum LOS deformation rate (~30 cm/yr estimated) stayed about constant during 2007–2011 (personal communication with Dr. Shi). However, between 2011 and 2016, the ~236 ± 19% increase in subsiding extent and ~177% increase in deformation rate are significant, which pose a threat to the safety of oil and gas facilities and other infrastructure. Our further discussion, therefore, focuses on finding the probable causes of such a large expansion and the acceleration of subsidence.

The groundwater level at well 4615924 (Fig. 1(b)), which is operated by Texas Water Development Board (TWDB) and located 3.5 km southwest of the Wink Sinks, exhibits seasonal fluctuation in the Cenozoic Pecos Alluvium aquifer: the water table rises in winter (a peak around January) and declines in summer (lowest between July and September) (Fig. 9(a)). This well, which provides continuous measurement of ground water level, only began operating in 2013, thus there are no records before 2013. Nearby, in downtown Kermit, the groundwater level has been annually measured in winter since the 1960s from two wells, 461602 and 4616103 (Fig. 1(b)). Measurements at both Kermit wells show the water table in the alluvium aquifer plummeting in 2011, recording the lowest water level in 30 years (Fig. 9(b)).

This area experiences seasonal variations in the water table due to the relatively high precipitation during spring and winter (Fig. 9(c)) and groundwater inflow from Delaware Basin and along the Capitan Reef (Fig. S4). However, there is little variation in the rate of time-series InSAR deformation (Fig. 6(b)), suggesting the deformation is essentially linear in time. Therefore, we find that the deformation around Wink Sinks is most likely independent of the seasonal fluctuation of groundwater. Although our InSAR measurements reported in this study span autumn to winter (period of high water table), our previous results (Kim et al., 2016) were acquired in summer (period of low water table), reaffirming that deformation in Wink Sinks and neighboring regions is temporally linear.

This area was hit by a severe to extreme state-wide drought in 2011, which might impact the stability of the subsurface and ground surface. The precipitation record from 1980 to 2016 (Fig. 9(c)) measured at a weather station (Fig. 1(b)) displays the lowest rainfall and the most severe drought in 2011 for at least 30 years (lowest rainfall since 1957 based on longer rainfall record). Only 4.92 cm of precipitation fell in the Wink area in 2011, just 16% of the 30-year annual average precipitation (31 cm) and 42% of the second lowest yearly rainfall in 1967 (11.61 cm). Such a significant decrease in precipitation can have an immediate and long-term negative impact on sinkhole-prone areas.

The Wink Sinks area has well-developed fracture systems in all layers from shallow to deep artesian aquifers (Heithecker, 1932; Adams, 1944; Baumgardner et al., 1982; Johnson, 1989). The record low precipitation and thereby lowered water table (Fig. 9 (b)) possibly influenced the existing fracture systems. A lowered water table can decrease the pore-fluid pressure and increase the effective stress (Terzaghi, 1925) of shale, sandstone, and dolomite (Fig. 10) in the

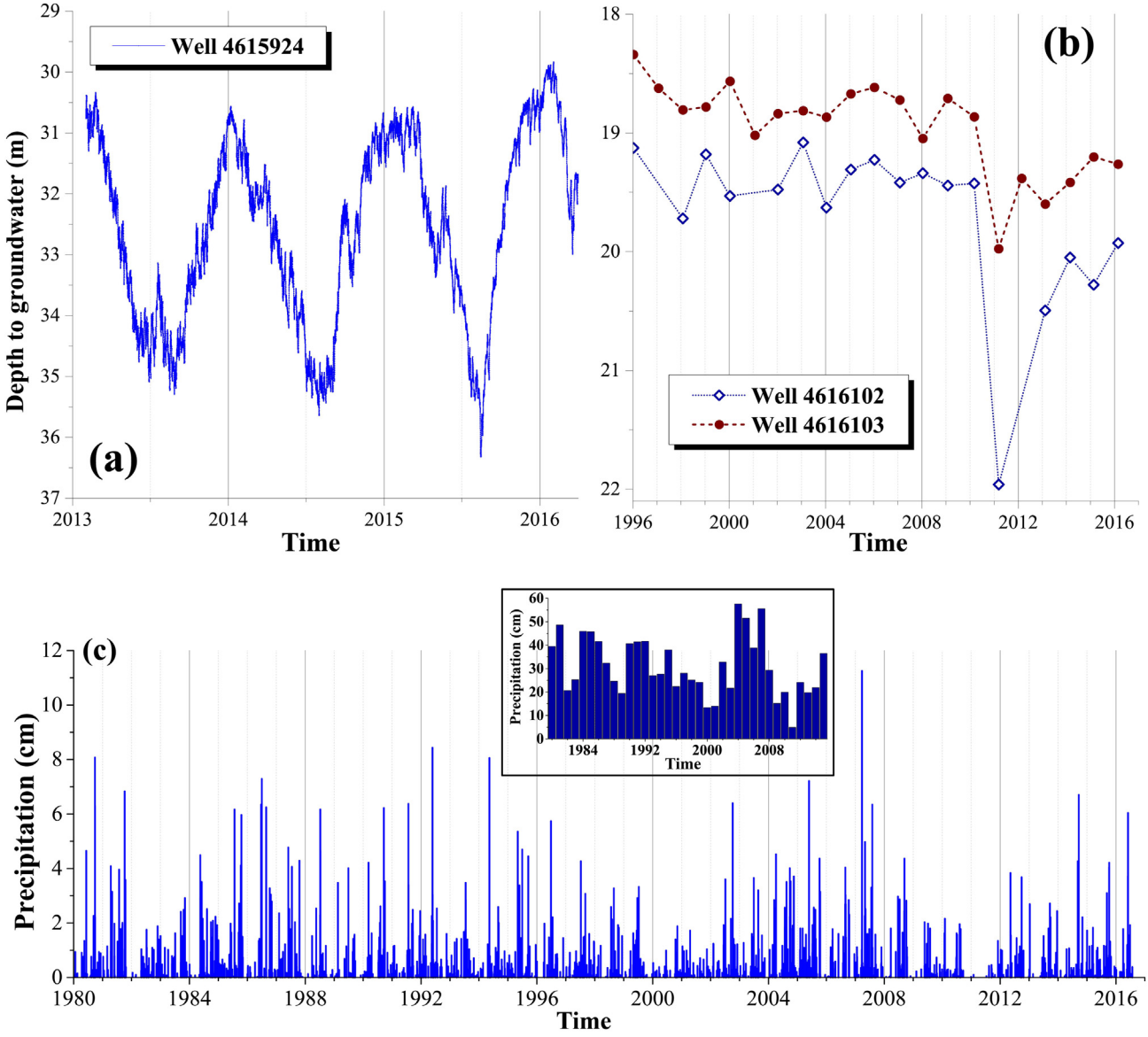

Fig. 9. (a) Daily groundwater level change at well 4615924 (blue triangle in Fig. 1(b)) from Feb 1, 2013 to Mar 31, 2016. (b) Annual groundwater level change at well 4616102 and 4616103 (blue triangles in Fig. 1(b)) since 1996. (c) Monthly precipitation at weather station (Fig. 1(b)) since January 1, 1980. Inset image represents yearly cumulative precipitation since 1980. (For interpretation of the references to colour in this figure legend, the reader is referred to the web version of this article.)

formations above and below the Salado Salt Bed. The rise of effective overburden stress can lead to fractures in the weakest part(s) of the formations. It is likely that the decadal water flooding operation (Fig. 8(b)) and pressurized water injection caused more fractures in the formations overlying and underlying the Salado Formation along with those formed during the borehole drilling and re-alignment. The rapid subsidence (Fig. 8(a)) has continued for a decade and the decadal surface displacement possibly led to the formation of rock fractures. The increased overburden stress of the strata due to the severe drought could widen the existing fractures and create more fractures. The resulting fractures can function as subsurface drainage pathways for fresh groundwater into the interbedded salt layer. Once groundwater level recovered from a severe drought, the downward freshwater flow from aquifers through fractures in formations overlying the Salado Formation and the upward freshwater flow from artesian aquifer through fractures in formations underlying the Salado Formation can accelerate pre-existing salt dissolution and result in more extensive cavity opening and larger surface subsidence (Fig. 10). The interplay between drought and opening of cavity has been a characteristic process of sinkhole development (Gutiérrez et al., 2014; Waltham et al., 2005) and the salt dissolution and transport mechanisms through rock fracture overlying the salt bed in Delaware Basin have been introduced by Wood et al. (1982) and reviewed by Davies (1984). A recent study on drought and sinkhole occurrence also witnessed a high correlation between severe drought periods and the temporal patterns of sinkhole development (Linares et al., 2017). Lowering groundwater causes an increase in the effective weight of cavity roofs by the loss of buoyant support from pore water. This may favor internal erosion processes by the replacement of slow phreatic flow by more rapid downward percolation, and may reduce the mechanical strength of deposits by desiccation and contraction (Lamoreaux and Newton, 1986; Gutiérrez et al., 2016; Linares et al., 2017). The ongoing subsidence (Fig. 8(a)) has not yet resulted in a collapse like Wink Sinks #1 and #2, however the characteristic feature in karst with such rapid subsidence rate can be classified as a cover-subsidence sinkhole (Gutiérrez et al., 2014).

Based on our observations, we propose that the widened subsurface

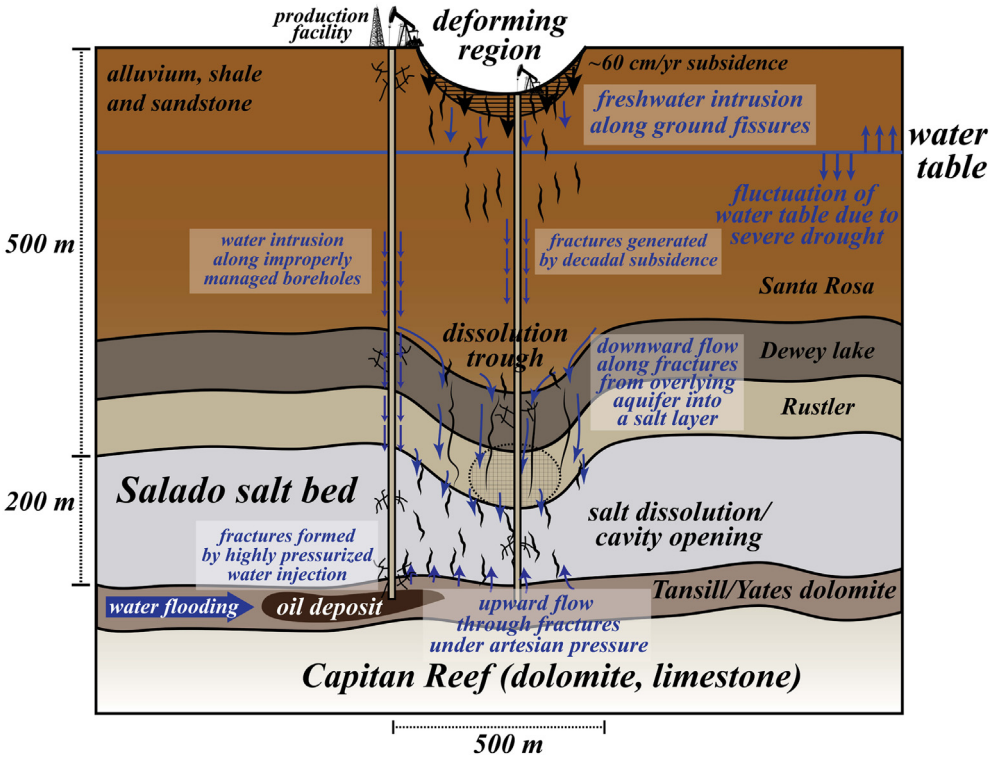

Fig. 10. Schematic figure (*not to scale*) of cross section along $\overline{\alpha\beta}$ in Fig. 5. Salado formation with ~200 m thickness is located at a depth of 500 m from surface. Severe drought and decline of water table increases the effective stress of rocks overlying the Salado formation, widens the existing fractures, and creates new fractures in formations as well as ground fissures on the surface. The fracture and ground fissures make vertical pathways for freshwater intrusion from rainfall, groundwater, and artesian aquifer into a salt layer and a salt dissolution finally opens the new cavity and results in the subsidence on the surface.

fracture networks may be a major contributor to the expansion of the subsiding area and the acceleration of the subsidence rate. However, our remote sensing methods using optical and radar imagery cannot confirm the existence of the fractures in the rock and soil column with 500–1000 m thickness. Instead, ground fissures can be one indicator to help infer the existence of such subsurface fractures, because ground fissures represent one kind of opened fracture formed as a result of soil surface tension due to severe drought and/or land subsidence (Singhal and Gupta, 2010). Both the InSAR coherence method, which delineates low coherence pixels from TerraSAR-X interferograms, and the optical imagery-based method, which draws lines with discontinuous surfaces from high-resolution Google Earth™ images, have enabled us to identify ground fissures (light blue lines in Fig. 8(a)) spreading over the subsiding areas. Many fissures developed on the subsiding area (Fig. 8(a)). Their existence was confirmed, as seen in photos of fissures (Fig. 11) from our September 2016 field trip to the most deforming area (region 'f' in Fig. 6(a)) around the intersection of County Road 201 and 204. These fissures were not reported by a previous field trip in 2008 (Paine et al., 2012). In addition, Google Earth™ images and aerial photography acquired before 2011 do not show their presence, but Google Earth™ imagery acquired in March 2013 clearly displays the fissures, suggesting they were created or widened as a result of large gradient of uneven subsidence as well as the influence of the severe drought in 2011. Moreover, due to the large subsidence and drought, the subsurface can also experience a similar process to create new fractures and widen the existing fractures in rock and soil layers that were generated as the consequence of hydrocarbon (water flooding) operations and improper borehole management (Singhal and Gupta, 2010; Zoback, 2007).

Our findings of ground fissures and overwhelming evidence of the presence of the fracture systems in the vicinity of the Wink Sinks (Heithecker, 1932; Adams, 1944; Johnson, 1989; Baumgardner et al., 1982; Lambert, 1983) suggest that the area, where the fracture systems are well developed, is rapidly subsiding. As with water flow paths created by poorly sealed or mismanaged boreholes and/or massive water production contributed to the collapse of Wink Sinks #1 and #2, the large deformation to the east of Wink Sink #2 may have similar origins. The opened fissures and fractures near the most deforming area made vertical pathways to the Salado Formation (Fig. 10), and the rapid salt dissolution was activated, causing the surface subsidence. However, unlike Wink Sinks #1 and #2, the subsidence has not (yet) led to a full collapse. Instead, before the 2011 drought, both the extent of subsidence and the rate of subsidence stayed constant for years. Once the water table recovered to pre-drought levels after severe droughts, more unsaturated water has been able to flow into the Salado Formation through well-developed fracture systems downward from the overlying aquifer system and upward from an underlying artesian aquifer. The salt dissolution in the salt beds resulted in the rapid surface subsidence (Fig. 10). Currently, no water flooding operations are in use around the peak subsiding area because only dry oil and gas have been produced since August 2008 (Fig. 8(b)). This excludes the possibility that the current expanded and accelerated subsidence after 2011 resulted from water flooding operations. However, when considering the onset and evolution of the subsidence sinkhole, the combined effect of both anthropogenic (borehole management, water control) and natural (fluctuation of water table due to a severe drought) causes contributed to the large deformation of ~53 cm/yr LOS deformation (~60 cm/yr subsidence).

The hypothesis that severe droughts can cause the acceleration of sinkhole occurrence has been long discussed despite the lack of direct observations (Waltham et al., 2005; Gutiérrez et al., 2014, 2016; Warren, 2016). Our InSAR-based observations exhibit the possibility of drought-driven sinkhole subsidence, which is in good agreement with a recent study on the high correlation between severe droughts and temporal patterns of sinkhole occurrence (Linares et al., 2017). Moreover, the seasonal changes of water table do not likely make an impact

Fig. 11. Photos taken in September 2016 of ground fissures (light blue lines in Fig. 8(a)) found around the intersection of County Road 201 and 204 (region 'f' along profile $\overline{AB}$ in Fig. 6(a)). The width of the fissures is ~10 cm. (For interpretation of the references to colour in this figure legend, the reader is referred to the web version of this article.)

on the existing fracture systems, based on the temporally linear subsidence independent of the seasonal effects. Instead, prolonged water table drop due to severe droughts can have irreversible effects on fracture systems (e.g., widening the fractures, creating more fractures and ground fissures), leading to accelerated subsidence in sinkhole-prone areas.

6. Conclusion

Oil, gas, and water production records and historical aerial photography indicate that the collapses of two sinkholes (Wink Sinks #1 and #2) in the past were closely related to hydrocarbon production activities, especially the massive water production associated with water flooding, during the oil boom era of the 1970s. Inappropriate borehole management and water control are main contributors to sinkhole collapses. Also, after the outcrop of Wink Sink #2, its vicinity continued to collapse and the sinkhole expanded until 2010. Hydrocarbon production around the Wink sinkholes has been abandoned or discontinued since 2005, possibly contributing to the relative stabilization of ground surface within Wink sinkholes.

Time-series InSAR measurements using high-resolution (~25 cm) staring spotlight TerraSAR-X revealed spatiotemporal details about the current status of the existing sinkholes and neighboring regions. Although the continuous collapse of Wink Sink #1 and #2 had ceased by 2010, the vicinities of the two sinkholes were still deforming in March 2016 at a rate ~5 cm/yr LOS displacement, which is possibly caused by mass-wasting and collapse processes filling the voids with superficial deposits. The deformation can be regarded as a result of

residual subsidence process, but a large subsidence of 53 cm/yr (in LOS direction) 1 km east of Wink Sink #2 near the intersection of County Road 201 and 204 poses a severe threat. We suggest that the initial trigger of the subsidence might be similar to that of Wink Sinks #1 and #2 (poor borehole management, water flooding operations in a karst environment), but the recent expanded and accelerated subsidence was likely induced by the severe drought in 2011. In an area with well-developed fracture systems such as Wink, drought can widen existing fractures and/or create new fractures in the rocks overlying and underlying the interbedded salt layer as well as the ground fissures on the surface. The fractures and ground fissures can open the pathways of freshwater from downward groundwater flow from aquifer, upward groundwater flow from artesian aquifer, and surface water flow, accelerating the salt dissolution and enlarging and creating the subsurface cavity. Therefore, the combined effects of human and natural perturbation can be responsible for the ongoing evolution of the subsidence sinkhole with a large deformation rate.

One last question from our study is: "*will the rapid ground subsidence turn into another collapse sinkhole*?" It is difficult to predict the future of this unstable surface. The subsiding area already underwent more than a10-year subsidence of tens of centimeter per year without collapse. We therefore cannot exclude the possibility that the rapid subsidence may be related to progressive dissolution of the Salado Formation and the concomitant bending of the overlying caprock without the creation of significant cavities and, in that case, the subsidence may not result in a collapse sinkhole. However, regardless of whether the ground surface fully collapses, rapid subsidence on the order of tens of centimeters per year can damage roads and nearby oil production facilities, contaminate water sources, and threaten the safe operation of pipelines transporting natural gas or hazardous liquid (Fig. 8(a)). To mitigate possible catastrophic outcomes, this area warrants continuous monitoring from federal and local authorities, petroleum and pipeline companies, and scientists. Finally, our methods of evaluating the development of existing and future sinkholes in Wink, Texas can be applied not only to the many existing sinkholes in the US and around the world, but also to areas where a sinkhole is in the earlier stages of formation, before collapse has occurred. These incipient sinkholes which cannot be detected by low-resolution remote sensing techniques can be possibly be identified by high-resolution imagery, thereby mitigating the geohazards and saving human lives.

Acknowledgements

This research was supported by NASA Earth Surface & Interior Program (NNX16AL10G), US Geological Survey Land Remote Sensing Program (G14AC00153), and the Shuler-Foscue Endowment at Southern Methodist University (SMU). Constructive comments from the Editor, three anonymous reviewers, and Cathy Chickering Pace improved the manuscript. Aerial photography was obtained through Geospatial Data Gateway of US Department of Agriculture, and the staring spotlight mode TerraSAR-X imagery were acquired upon the data request to the German Aerospace Center (DLR) (GEO2462). The oil/gas/water production information was gathered through the Texas RRC and drillinginfo™ database with the aid of Maria Richards in the SMU Geothermal Lab. Groundwater data were acquired from the Texas Water Development Board (TWDB) water science and conservation group. Geocoded figures were drawn by general mapping tools (GMT).

Appendix A. Supplementary data

Supplementary data to this article can be found online at https://doi.org/10.1016/j.rse.2018.12.028.

References

Carrara, W.G., Goodman, R.S., Majewski, R.M., 1995. Spotlight Synthetic Aperture Radar. Artech House, Norwood, MA, USA.
Abelson, M., Yechieli, Y., Crouvi, O., Baer, G., Wachs, D., Bein, A., Shtivelman, V., 2006. Evolution of the Dead Sea sinkholes. Geol. Soc. Am. Spec. Pap. 401, 241–253.
Ackers, A.L., DeChicchis, R., Smith, R.H., 1930. Hendrick Field, Winkler County, Texas. Am. Assoc. Pet. Geol. Bull. 14, 923–944.
Adams, J.E., 1944. Upper Permian Ochoan Series of Delaware Basin, west Texas and southeastern New Mexico. Am. Assoc. Pet. Geol. Bull. 28, 1596–1625.
Anderson, R.Y., 1981. Deep-seated salt dissolution in the Delaware Basin, Texas and New Mexico. In: New Mexico Geological Society, Special Publication No. 10, pp. 133–145.
Anderson, R.Y., Kirkland, D.W., 1980. Dissolution of salt deposits by brine density flow. Geology 8, 66–69.
Anderson, R.Y., Kietzke, K.K., Rhodes, D.J., 1978. Development of dissolution breccias, northern Delaware Basin, New Mexico and Texas. In: New Mexico Bureau Mines & Mineral Resources. Circular 159. pp. 47–52.
Atzori, S., Antonioli, A., Salvi, S., Baer, G., 2015. InSAR-based modeling and analysis of sinkholes along the Dead Sea coastline. Geophys. Res. Lett. 42, 8383–8390.
Avni, Y., Lensky, N., Dente, E., Shviro, M., Arav, R., Gavrieli, I., Yechieli, Y., Abelson, M., Lutzky, H., Filin, S., Haviv, I., Baer, G., 2016. Self-accelerated development of salt karst during flash floods along the Dead Sea Coast, Israel. J. Geophys. Res. Earth Surf. 121, 17–38.
Bachman, G.O., 1976. Cenozoic deposits of southeastern New Mexico and an outline of the history of evaporite dissolution. US Geol. Surv. J. Res. 4 (2), 135–149.
Baer, G., Schattner, U., Wachs, D., Sandwell, D., Wdowinski, S., Frydman, S., 2002. The lowest place on Earth is subsiding—an InSAR (interferometric synthetic aperture radar) perspective. Geol. Soc. Am. Bull. 114 (1), 12–23.
Baumgardner, R.W., Hoadley, A.D., Goldstein, A.G., 1982. The Wink Sinks; a case history of evaporite dissolution and catastrophic subsidence: Formation of the Wink Sink, a salt dissolution and collapse feature, Winkler County, Texas. In: Bureau of Economic Geology, The University of Texas at Austin, Report of Investigations No. 114, (38 p).
Berardino, P., Fornaro, G., Lanari, R., Sansosti, E., 2002. A new algorithm for surface deformation monitoring based on small baseline differential SAR interferograms. IEEE Trans. Geosci. Remote Sens. 40, 2375–2383.
Castañeda, C., Gutiérrez, F., Manunta, M., Galve, J.P., 2009. DInSAR measurements of ground deformation by sinkholes, mining subsidence, and landslides, Ebro River, Spain. Earth Surf. Process. Landf. 34, 1562–1574.
Chang, L., Hanssen, R.F., 2014. Detection of cavity migration and sinkhole risk using radar interferometric time series. Remote Sens. Environ. 147, 56–64.
Closson, D., Karaki, N.A., Hussein, M.J., Al-Fugha, H., Ozer, A., 2003. Space-borne radar interferometric mapping of precursory deformations of a dyke collapse, Dead Sea area, Jordan. Int. J. Remote Sens. 24, 843–849.
Closson, D., Karaki, N.A., Klinger, Y., Hussein, M.J., 2005. Subsidence and sinkhole hazards assessment in the southern Dead Sea area, Jordan. Pure Appl. Geophys. 162, 221–248.
Crabtree, M., Romano, C., Tyrie, J., Elphick, J., Kuchuk, F., Romano, C., Roodhart, L., 2000. Water Control, Oilfield Review. 12(1). pp. 30–51.
Davies, P.B., 1984. Deep-seated Dissolution and Subsidence in Bedded Salt Deposits (Doctoral thesis). Stanford University.
Dean, W.E., Johnson, K.S., 1989. Anhydrite deposits of the United States and characteristics of anhydrite important for storage of radioactive wastes. U.S. Geol. Surv. Prof. Pap. 1794 (132 p).
Filin, S., Baruch, A., Avni, Y., Marco, S., 2011. Sinkhole characterization in the Dead Sea area using airborne laser scanning. Nat. Hazards 58, 1135–1154.
Fleury, S., 2009. Land Use Policy and Practice on Karst Terrains: Living on Limestone. Springer, Netherlands. https://doi.org/10.1007/978-1-4020-9670-9. (187 p.).
Gutiérrez, F., Galve, J.P., Lucha, P., Cadtañeda, C., 2012. Integrating geomorphological mapping, trenching, InSAR and GPR for the identification and characterization of sinkholes: a review and application in the mantled evaporite karst of the Ebro Valley (NE Spain). Geomorphology 134, 144–156.
Gutiérrez, F., Parise, M., De Waele, K., Jourde, H., 2014. A review on natural and human-induced geohazards and impacts in karst. Earth Sci. Rev. 138, 61–88.
Gutiérrez, F., Fabregat, I., Roqué, C., Carbonel, D., Guerrero, J., García-Hermoso, F., Zarroca, M., Linares, R., 2016. Sinkholes and caves related to evaporite dissolution in a stratigraphically and structurally complex setting, Fluvia Valley, eastern Spanish Pyrenees. Geological, geomorphological and environmental implications. Geomorphology 267, 76–97.
Heithecker, R.E., 1932. Some methods of separating oil and water in west Texas fields, and the disposal of oil-field brines in the Hendrick Oil Field, Texas. In: U.S. Bur. Mines Rept. Of Investig. 3173. 16.
Hill, C.A., 2003. Intrastratal karst at the waste isolation pilot plant site, Southeastern New Mexico. In: Oklahoma Geological Survey, Circular. 109. Oklahoma Geological Survey, Norman, OK, USA, pp. 197–209.
Hills, J.M., 1970. Late Paleozoic structural directions in southern Permian Basin, west Texas and New Mexico. Am. Assoc. Pet. Geol. Bull. 54, 1809–1827.
Hills, J.M., 1984. Sedimentation, tectonism, and hydrocarbon generation in Delaware Basin, West Texas and southeastern New Mexico. Am. Assoc. Pet. Geol. Bull. 68 (3), 250–267.
Hiss, W.L., 1980. Movement of ground water in Permian Guadalupian aquifer systems, southeastern New Mexico and Western Texas. In: New Mexico Geological Society Guidebook, 31st Field Conference, Trans-Pecos Region, pp. 289–294.
Johnson, K.S., 1986. Salt Dissolution and Collapse at the Wink Sink in West Texas. Office of Nuclear Waste Isolation, Battelle Memorial Institute, Columbus, OH (BMI/ONWI-598, 83 p).
Johnson, K.S., 1989. Development of the Wink Sink in west Texas, U.S.A., due to salt dissolution and collapse. Environ. Geol. Water Sci. 14 (2), 81–92.
Johnson, K.S., 2005. Subsidence hazards due to evaporite dissolution in the United States. Environ. Geol. 48, 395–409.

Johnson, K.S., Collins, E.W., Seni, S.J., 2003. Sinkholes and land subsidence due to salt dissolution near Wink, West Texas, and other sites in western Texas and New Mexico. In: Oklahoma Geological Survey, Circular. 109. Oklahoma Geological Survey, Norman, OK, USA, pp. 183–195.

Jones, C.E., Blom, R.G., 2014. Bayou Corne, Louisiana, sinkhole: precursory deformation measured by radar interferometry. Geology 42, 111–114.

Jónsson, S., Zebker, H., Segall, P., Amelung, F., 2002. Fault slip distribution of the 1999 Mw 7.1 Hector Mine earthquake, California, estimated from satellite radar and GPS measurements. Bull. Seismol. Soc. Am. 92, 1377–1389.

Kim, J.-W., Lu, Z., 2018. Association between localized geohazards in West Texas and human activities, recognized by Sentinel-1A/B satellite radar imagery. Sci. Rep. 8, 4727. https://doi.org/10.1038/s41598-018-23143-6.

Kim, J.-W., Lu, Z., Degrandpre, K., 2016. Ongoing deformation of sinkholes in Wink, Texas, observed by time-series Sentinel-1A SAR interferometry (preliminary results). Remote Sens. 8, 313.

Kirkland, D.W., Evans, R., 1976. Origin of limestone buttes, Gypsum Plain, Culberson County, Texas. In: The American Association of Petroleum Geologists Bulletin. 60. pp. 2005–2018.

Kobal, M., Bertoncelj, I., Pirotti, F., Dakskobler, I., Kutnar, L., 2015. Using Lidar data to analyse sinkhole characteristics relevant for understory vegetation under forest cover-case study of a high karst area in the Dinaric mountains. PLoS One 10 (3), e0122070. https://doi.org/10.1371/journal.pone.0122070.

Kraus, T., Bräutigam, B., Mittermayer, J., Wollstadt, S., Grigorov, C., 2016. TerraSAR-X staring spotlight mode optimization and global performance predictions. IEEE J. Sel. Top. Appl. Earth Observ. Remote Sens. 9 (3), 1015–1027.

Kuniansky, E.L., Weary, D.J., Kaufmann, J.E., 2016. The current status of mapping karst areas and availability of public sinkhole-risk resources in karst terrains of the United States. Hydrogeol. J. 24, 613–624.

Lambert, S.J., 1983. Dissolution of Evaporites in and Around the Delaware Basin, Southeastern New Mexico and West Texas. Sandia National Laboratories, Albuquerque, NM (SAND82-0461).

Lamoreaux, P.E., Newton, J.G., 1986. Catastrophic subsidence: an environmental hazard, Shelby County, Alabama. Environ. Geol. Water Sci. 8, 25–40.

Land, L., 2003. Evaporite karst and regional ground-water circulation in the Lower Pecos Valley of Southeastern New Mexico. In: Oklahoma Geological Survey, Circular. 109. Oklahoma Geological Survey, Norman, OK, USA, pp. 227–232.

Land, L., 2013. Geophysical records of anthropogenic sinkhole formation in the Delaware Basin region, Southeast New Mexico and West Texas, USA. Carbonates Evaporites 28 (1), 183–190.

Linares, R., Roqué, C., Gutiérrez, F., Zarroca, M., Carbonel, D., Bach, J., Fabregat, I., 2017. The impact of droughts and climate change on sinkhole occurrence. A case study from the evaporite karst of the Fluvia Valley, NE Spain. Sci. Total Environ. 579, 345–358.

Lu, Z., Dzurisin, D., 2014. InSAR imaging of Aleutian volcanoes: monitoring a volcanic arc from space. In: Springer Praxis Books, Geophysical Sciences. Springer (390 pp).

Lu, Z., Wicks Jr., C., 2010. Characterizing 6 August 2007 Crandall Canyon mine collapse from ALOS PALSAR InSAR. Geomat. Nat. Haz. Risk 1, 85–93.

Maley, V.L., Huffington, R.M., 1953. Cenozoic fill and evaporite solution in the Delaware Basin, Texas and New Mexico. Geol. Soc. Am. Bull. 64, 539–546.

Nof, R.N., Baer, G., Ziv, A., Raz, E., Atzori, S., Salvi, S., 2013. Sinkhole precursors along the Dead Sea, Israel, revealed by SAR interferometry. Geology 41 (9), 1019–1022.

Okada, Y., 1985. Subsurface deformation due to shear and tensile faults in a half-space. Bull. Seismol. Soc. Am. 92 (2), 1018–1040.

Paine, J.G., Buckley, S.M., Collins, E.W., Wilson, C.R., 2012. Assessing collapse risk in evaporite sinkhole-prone areas using microgravimetry and radar interferometry. J. Environ. Eng. Geophys. 17, 75–87.

Panno, S.V., Luman, D.E., 2012. Mapping Palimpsest karst features of Illinois' sinkhole plain using historical aerial photography. Carbonates Evaporites 28 (1–2), 201–214.

Powers, D.W., 2003. Jal sinkhole in southeastern New Mexico – evaporite dissolution, drill holes, and the potential for sinkhole development. In: Johnson, K.S., Neal, J.T. (Eds.), Evaporite Karst and Engineering/environmental Problems in the United States. Oklahoma Geological Survey Circular 109. Oklahoma Geological Survey, Norman, OK, USA, pp. 219–226.

Powers, D.W., Lambert, S.J., Shaffer, S.E., Hill, L.R., Weart, W.D., 1978. Geological Characterization Report, Waste Isolation Pilot Plant (WIPP) Site, Southeastern New Mexico. vol. 2 Sandia Laboratories, Albuquerque, NM, SAND78-1596.

Qu, F., Lu, Z., Zhang, Q., Bawden, G.W., Kim, J.-W., Zhao, C., Qu, W., 2015. Mapping ground deformation over Houston-Galveston, Texas using multi-temporal InSAR. Remote Sens. Environ. 169, 290–306.

Rucker, M.L., Panda, B.B., Meyers, R.A., Lommler, J.C., 2013. Using InSAR to detect subsidence at brine wells, sinkhole sites, and mines. Carbonates Evaporites 28 (1), 141–147.

Samsonov, S.V., González, P.J., Tiampo, K.F., d'Oreye, N., 2014. Modeling of fast ground subsidence observed in southern Saskatchewan (Canada) during 2008–2011. Nat. Hazards Earth Syst. Sci. 14, 247–257.

Schmidt, D.A., Bürgmann, R., 2003. Time-dependent land uplift and subsidence in the Santa Clara valley, California, from a large interferometric synthetic aperture radar dataset. J. Geophys. Res. 108 (B9), 2416. https://doi.org/10.1029/2002JB002267.

Seale, L.D., Florea, L.J., Vacher, H.L., Brinkmann, R., 2008. Using ALSM to map sinkholes in the urbanized covered karst of Pinellas County, Florida-1, methodological considerations. Environ. Geol. 54, 995–1005.

Singhal, B.B.S., Gupta, R.P., 2010. Applied Hydrogeology of Fractured Rocks, second edition. Springer, Netherland. https://doi.org/10.1007/978-90-481-8799-7. (408 p).

Standen, A., Finch, S., Williams, R., Lee-Brand, B., 2009. Capitan Reef complex structure and stratigraphy. Texa Water Development Board, Contract Number 0804830794. (53 p).

Terzaghi, K., 1925. Erdbaumechanik auf Bodenphysikalischer Grundlage. Franz Deuticke, Liepzig-Vienna.

Vance, M., 1928. Development and production methods in west Texas. Oil Weekly 50 (1), 34–44.

Waltham, T., Bell, F.G., Culshaw, M., 2005. Sinkholes and subsidence: karst and cavernous rocks in engineering and construction. In: Springer-Praxis Books in Geophysical Sciences. Springer, Heidelberg, Germany.

Warren, J.K., 2016. Evaporites: A Geological Compendium, 2nd edition. Springer (1813 p).

Weary, D.J., 2015. The cost of karst subsidence and sinkhole collapse in the United States compared with other natural hazards. In: Doctor, D.H., Land, L., Stephenson, J.B. (Eds.), Sinkholes and the Engineering and Environmental Impacts of Karst, Proceedings of the Fourteenth Multidisciplinary Conference, October 5–9, Rochester, Minnesota: NCKRI Symposium 5. National Cave and Karst Research Institute, Carlsbad (NM), pp. 433–445. Available at: http://scholarcommons.usf.edu/sinkhole_2015/ProceedingswithProgram/Mgmt_Regs_Education/1.

Wood, B.J., Snow, R.E., Cosler, D.J., Haji-Djafari, S., 1982. Delaware Mountain Group (DMG) Hydrology – Salt Removal Potential. 3166 U.S. Department of Energy TME (136 p).

Zhu, J., Pierskalla Jr., W.P., 2016. Applying a weighted random forests method to extract karst sinkholes from LiDAR data. J. Hydrol. 533, 343–352.

Zhu, J., Taylor, T.P., Currens, J.C., Crwford, M.M., 2014. Improved karst sinkhole mapping in Kentucky using LiDAR techniques: a pilot study in Floyds Fork Watershed. J. Cave Karst Stud. 76 (3), 207–216.

Zoback, M.D., 2007. Reservoir Geomechanics. Cambridge University Presshttps://doi.org/10.1017/CBO9780511586477. 452 p.